Structural Engineering and Mechanics, Vol. 21, No. 4 (2005) 393-406
DOI: http://dx.doi.org/10.12989/sem.2005.21.4.393

Experimental study on the deformation characteristics of RC beam-column subassemblages

Zixiong Guo† and Yong Yang‡

College of Civil Engineering, Huaqiao University, Quanzhou 362021, China

(Received June 14, 2004, Accepted August 12, 2005)

Abstract. Cyclic loading tests were carried out on six half-scale reinforced concrete beam-column subassemblages designed to the current Chinese Seismic Design Code for Buildings. The deformation behavior and restoring force characteristics of the subassemblages were studied. Emphasis was directed on their seismic behavior and deformation components. Based on test data and a simplified analysis model of the global and local deformation, the contribution of the deformation components due to beam flexure, column flexure, joint shear, and slippage of longitudinal reinforcement in the joint to the global deformation of subassemblages at different displacement amplitudes of cyclic loading was investigated.

Key words: reinforced concrete; beam-column subassemblage; seismic behavior; deformation characteristics.

1. Introduction

The inelastic deformation response of a RC structure during a strong earthquake is not caused by flexure alone. Many experimental investigations have indicated that the global inelastic displacement of a reinforced concrete (RC) structure is mainly a combination of flexural and shear deformation in critical regions, bond-slip of reinforcing bars in beam-column joints, and shear deformation in joint cores. The contribution of each of these deformation components to the global deformation is relative to the geometrical conditions, loading conditions (composition of loads and loading history), and reinforcement characteristics of the RC members. Cyclic loading tests on RC specimens with small shear span ratios indicated that deformations due to inelastic shear effects can be up to or in excess of 40% of the plastic hinge region deformation when under large deformation reversals (Fenwick *et al.* 1996). Measurements obtained from a series of beam and column tests also indicated that the displacement due to bond-slip of reinforcing bars in the beam-column joint is one of the major components of inelastic deformation (Saatcioglu *et al.* 1992).

To date, the available knowledge on the hysteretic model of all the deformation components noted above is incomplete. In the state of the art on seismic response analyses of RC structures, only the hysteretic behavior of a flexural component can be reasonably modeled. For a more rational analysis of the seismic response of RC structures, further research on each deformation component

† Professor, Corresponding author, E-mail: guozxcy@hqu.edu.cn
‡ PhD

and their hysteretic characteristics is required.

The inter-story drift of a RC frame structure is due to a combination of the deformations of beams, columns and joints in the story considered. Accordingly, experimental studies on isolated beam or column units are unable to properly represent the global deformation behavior of RC frames. Only those tests on beam-column subassemblages can reasonably represent the inter-story deformation behavior of a RC frame. Though a wealth of experimental studies on RC frame joints has been reported during the last three decades (Paulay 1988, Attaalla and Agbabian 2003), it should be noted that the focus of these studies was the shear strength of joint cores and the anchorage behavior of longitudinal bars in joint cores. However, the main purpose of beam-column subassemblage tests is to establish the deformation capacity relationship between subassemblage and global frames.

Some experimental investigations on RC beam-column subassemblages have been reported in the past. Bertero and Popov (1977) pointed out that the mechanical model of frame elements should include not only the change in the observed monotonically pseudo-static inelasticity of the material, but also the degradation in stiffness caused by cyclic loading reversals as a consequence of: (a) high shear; (b) bond degradation; and (c) slippage of the bars in joint, based on a series of experimental studies on subassemblages. Zerbe and Durrani (1989) studied the effect of the presence of a floor slab on the behavior of beam-column connections by testing two-bay frame subassemblages. Teraoka *et al.* (1998) studied the ductility performance and restoring force characteristics of interior frame subassemblages using high-strength materials based on fourteen half-scale interior beam-column subassemblages. Quintero-Febres and Wight (2002) conducted an experimental investigation to evaluate the response of interior wide beam-column connections to earthquake-type lateral loading in terms of the bond behavior of the longitudinal reinforcement, joint shear behavior, beam plastic hinge spreading, and slab participation.

The reliability of a dynamic inelastic analysis of reinforced concrete structures depends to a great extent on the hysteretic modeling of structural components. The tests of beam-column subassemblages mentioned above indicate that the total displacement of a subassemblage under cyclic loading consists of components due to flexure, shear, and slippage of longitudinal reinforcement in a joint. Though intensive efforts have been made to formulate the analytical model for the simulation of the hysteretic behavior of reinforced concrete subassemblages (Teraoka *et al.* 1996, Shin and Lafave 2004), further study is still needed to accurately take into account all these deformation components in an analytical model and to make it more applicable. To achieve this objective, the rational quantification of the contribution of all these various deformation components to the overall displacement is needed.

The main objectives of the present experimental study are as follows: (1) to obtain information on strength, ductility, deformation characteristics, hysteretic characteristics, drift capacity, and mechanisms of failure occurring in the critical regions of subassemblages of reinforced concrete structures when subjected to severe cyclic loading; (2) to obtain information on the contribution of the deformation components due to beam flexure, column flexure, joint shear, and slippage of longitudinal reinforcement in the joint to the global deformation, respectively, in those weak beam-strong column subassemblages at different displacement amplitudes of cyclic loading; and (3) to assess the seismic design implications of the obtained test results and to make suggestions for improving the current Chinese Seismic Design Code for Buildings.

2. Experimental procedure

2.1 Test specimens and experimental setup

The seismic behavior and deformation components of general RC frames were investigated by testing six 1/2-scale RC beam-column subassemblages. The subassemblage represented the typical unit of a multistory frame between the points of inflection (Fig. 1). The columns had a 200-mm square cross-section and the beams had a cross-section of 150 mm × 250 mm. The subassemblages were designed to develop flexural yielding of the beam prior to flexural yielding of the column. Table 1 shows the material properties of concrete and reinforcement, respectively. Fig. 2 and Table 2 show the geometric and sectional characteristics of the test specimens.

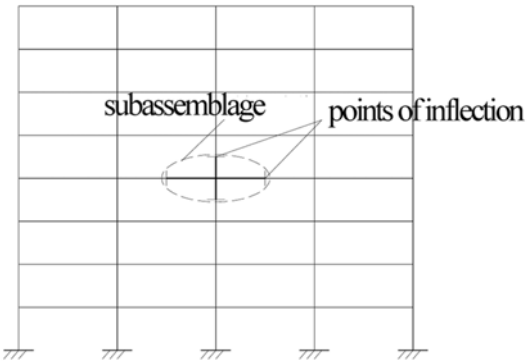

Fig. 1 Typical beam-column subassemblage in a frame

Table 1 Material properties of specimens

Specimens	Concrete		Reinforcement				
	f_{cu} (MPa)	E_c (MPa)	Diameter (mm)	f_y (MPa)	f_u (MPa)	E_s (MPa)	ε_y ($\mu\varepsilon$)
SP1~SP3	35.7	3.05×10^4	Φ12	360.2	528.2	1.70×10^5	2120
SP4~SP6	36.0	3.53×10^4	Φ6.2	350	493.5	2.05×10^5	1683
			Φ4		640.6		

Table 2 Reinforcement details of test subassemblages

Specimen	Reinforcement			
	① column bars	② beam bars	③ beam stirrups	④ joint stirrups (η_{cb})
SP1	8Φ12	2Φ12	Φ4@60	2Φ6+3Φ4@60(1.50)
SP2	8Φ12	2Φ12	Φ6@70	2Φ6+3Φ4@60(1.50)
SP3	8Φ12	2Φ12	Φ6@50	2Φ6+3Φ4@60(1.50)
SP4	8Φ12	3Φ12	Φ6@70	2Φ6+3Φ4@60(1.00)
SP5	8Φ12	3Φ12	Φ6@70	4Φ6@70 (1.11)
SP6	8Φ12	3Φ12	Φ6@70	6Φ6@45 (1.33)

Note: η_{cb} was the strength ratio of joint to beam and column.

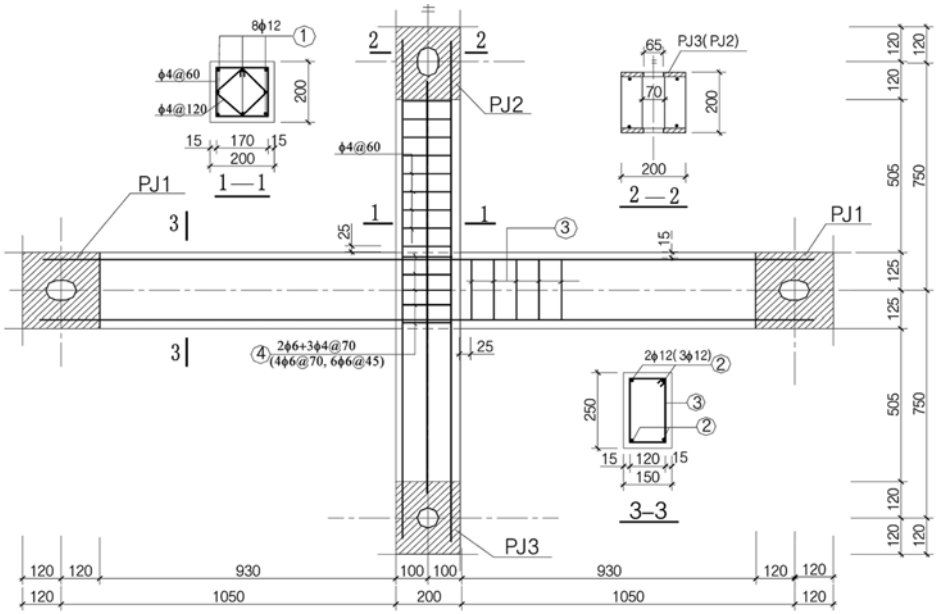

Fig. 2 Sectional characteristics and reinforcement details of specimens

2.2 Test loading setup

Axial load was applied to the column end of a subassemblage by a vertical jack and a large steel beam on the top of the loading shelf, and a horizontal load was imposed by a SCHENCK electronic servo-load system. The test setup is shown in detail in Fig. 3. In order to simulate the deformation more accurately and considering the P-Δ effect existing in real frame structures, equipment to ensure free deformation of the column was used (Fig. 3). By employing sixteen rolling bearings on the four corners of the loading shelf, the effect of friction was significantly reduced during the

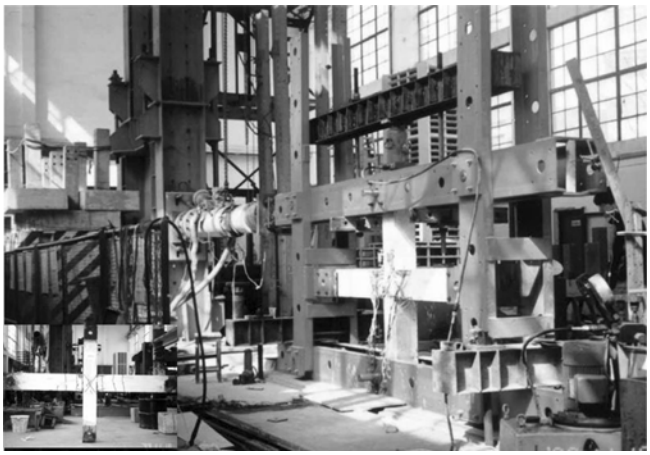

Fig. 3 Test loading setup

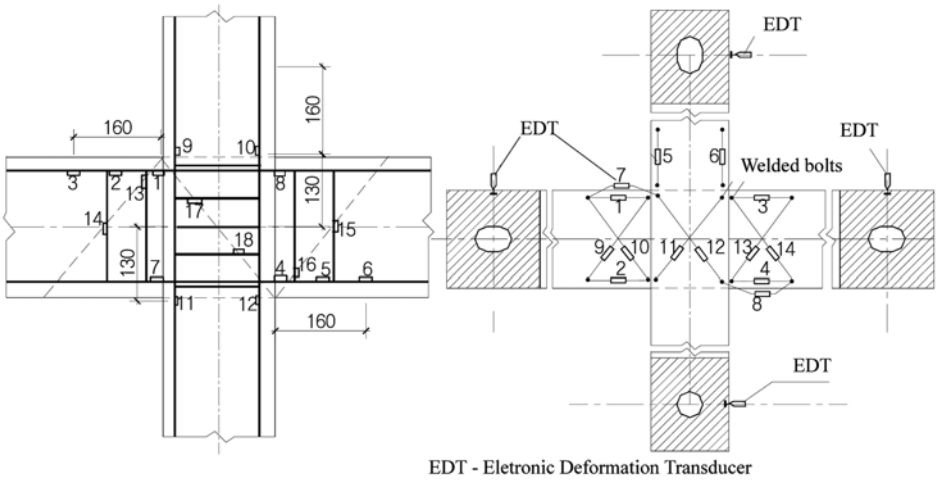

(a) Strain gauges (b) Deformation transducers

Fig. 4 Layout of the strain gauges and instruments

experiment. The experiment was carried out in the State Key Laboratory for Disaster Reduction in Civil Engineering of TongJi University.

2.3 Measured contents and instruments

The main results that could be obtained from this test are as follows: (1) the displacements of both the subassemblages and the supports, which are measured by electronic displacement transducers; (2) the flexural and shear deformation in plastic-hinge regions, bond-slip of reinforcing bars in the beam-column joint, and shear deformation in the joint core, which are obtained by electronic deformation transducers; and (3) the strains of longitudinal reinforcing bars and stirrups in the critical regions, which are measured by electronic resistor strain gauges. The detailed layout of all the measuring instruments and the strain gauges is shown in Fig. 4. In Fig. 4, the strain gauges of the stirrups are located according to the dotted lines, and the dip angle of the dotted line in the beam end is 45 degrees. The location of the strain gauges in the joint core region is denoted by the diagonal line.

2.4 Loading procedure

First, the predetermined axial load was applied to the column, and then the transverse load was applied. The axial load was held constant during the application of the transverse load. The horizontal loading process was controlled by both the force method and displacement method. The detailed processes were as follows: (1) Before the specimens yielded, the load was applied with a force control, with one cyclic repeat at each load level of $0.8P_y'$, $0.9P_y'$, $1.0P_y'$, $1.1P_y'$, $1.2P_y'$, … , where P_y' was the estimated yielding load. If any strains of the longitudinal reinforcing bars on the tension reign of the beams were found to have attained the yield strain, the loading procedure was stopped and then the yielding displacement Δ_y as well as the yielding load P_y were recorded.

(2) After yielding, the horizontal load was applied according to the yielding displacement Δ_y, and at each displacement level of Δ_y, $2\Delta_y$, $3\Delta_y$, $4\Delta_y$, $5\Delta_y$……, three loading cycles were performed. The whole loading procedure finished when the bearing capacity of the specimen was reduced to 80% of the maximum load value (P_{max}) or the hysteretic curves appeared unstable.

3. Test results

3.1 Final failure modes

In the tests, although all the subassemblages reached their maximum bearing capacity after the beam end yielded, the final failure modes varied according to the change of stirrup amount in the joint core (Fig. 5). For those specimens SP1, SP2, and SP3, whose strength ratio of joint to beam and column, η_{cb}, is equal to 1.50, the final failure modes were typical beam end bending failure mode, and small cracks occurred in the joint core region (Fig. 5a). For specimen SP6, η_{cb} = 1.33, although the joint core cracked more severely than the above three specimens, its failure mode could also be regarded as beam end bending failure mode, because its bending cracks were also mainly concentrated in the beam end (Fig. 5d).

For specimen SP5, η_{cb} = 1.10, many of the inclined cracks in the joint core region developed quickly after yielding of the longitudinal reinforcing bars in the beam end, and a net-shape inclined crack pattern was finally formed. At the displacement level $4\Delta_y$, the maximum width of

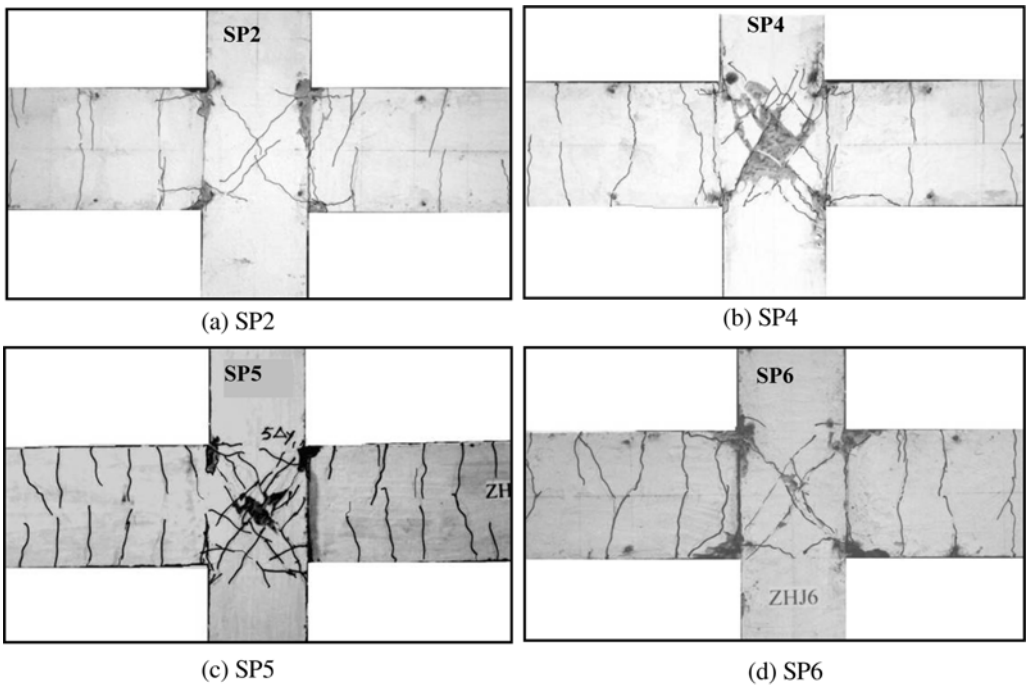

Fig. 5 Ultimate failure modes (local)

the diagonal cracks in the joint core region was up to 1.0 mm, and the concrete cover of the joint core was severely crushed and spalled off. The plastic deformation of specimen SP5 was mainly focused in the beam end and the joint core region, and the final failure mode could be regarded as a combination failure mode of the beam end bending failure and joint core shear failure mode (Fig. 5c).

For specimen SP4, η_{cb} = 1.0, when the longitudinal reinforcing bars at the beam end yielded, a series of parallel inclined cracks appeared in the joint core simultaneously. With increasing displacement amplitude, the shearing cracks in the joint core region developed more rapidly than the bending cracks at the end of the beam. When the displacement amplitude exceeded $4\Delta_y$, a distinctly lateral expansion deformation in the whole joint region was observed, and the width of the inclined crack of the joint core increased during the cyclic loading under the same displacement amplitude. At the same time, the development of bending cracks at the end of the beam was stable, except for critical cracks at the interface of the beam and the column, which were caused by bond-anchorage failure of the longitudinal reinforcing bars in the joint core region (Fig. 5b).

3.2 Yielding of the reinforcing bars and stirrups

The measured values of the reinforcing bar strains, which were recorded and displayed with a computer, could be easily checked during the whole test procedure. With increasing displacement amplitude, all the strains of longitudinal bars in the beam attained their yielding strain values gradually while none of the strain values of longitudinal bars in the column reached its yielding value. The strain values of the stirrups in the joint core region depended on the level of shear force transferred to the joint and the amount of the stirrups.

The stirrup strains in the joint core region developed in good agreement with the global failure mode of the subassemblage. The strain values of stirrups in the joint core increased abruptly as soon as inclined cracks in the joint core region occurred. Fig. 6 shows different relationships of story shear and joint stirrup strain for joints with different amount of stirrups in the joint core region of the subassemblages.

From Fig. 6(a), the stirrups strain of specimen SP4 (η_{cb} = 1.0) attained yield at a displacement level of $2\Delta_y$, and increased with the development of displacement amplitude. When the strain values of all of the stirrups in the joint core reached yield strains, the degree of damage in the joint core

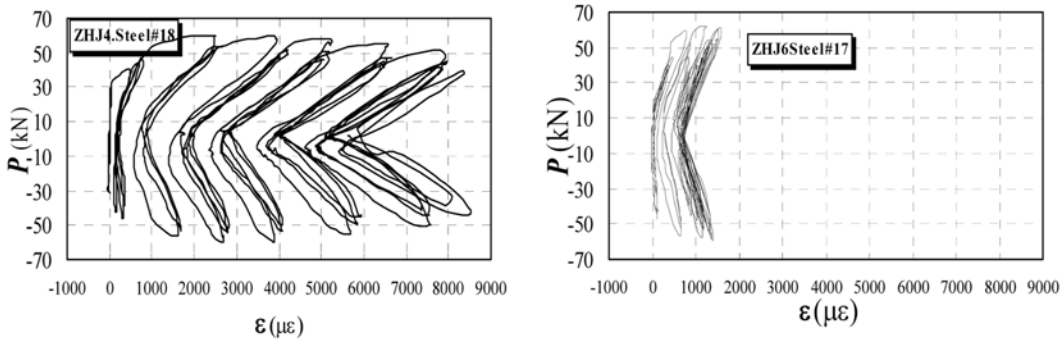

(a) SP4 (η_{cb}=1.0) (b) SP6 (η_{cb}=1.33)

Fig. 6 Relationships of story shear and joint stirrups strain

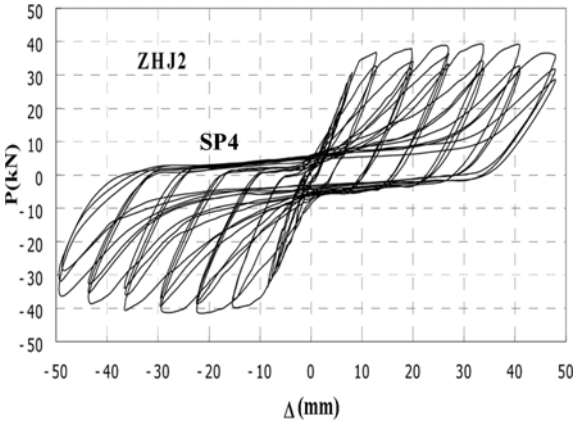

Fig. 7 P-Δ Hysteretic relationships

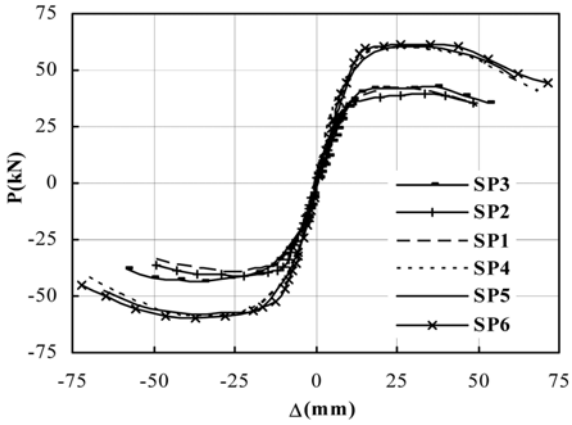

Fig. 8 Skeleton curve

increased, and the final failure mode of the specimen became joint shear failure.

Although specimen SP5 (η_{cb} = 1.10) was designed to be a strong-joint-weak-beam subassemblage according to the current *Chinese Seismic Design Code for Buildings*, the stirrups in the joint core region all yielded eventually because of the post-yield strengthening of bending bearing capacity at the beam end. For specimen SP6 (η_{cb} = 1.33), the stirrups in the joint core still remained in the linear elastic range when this specimen reached its ultimate failure (Fig. 6b).

3.3 Hysteretic characteristic and the skeleton curves

A typical hysteretic curve is shown in Fig. 7. In the high displacement range above a displacement amplitude of $5\Delta_y$, an increase in the amount of stirrups in the beam end and joint core region leads to a reduction in strength degradation, and softening of the hysteretic loop is postponed.

By comparing the P-Δ curves shown in Fig. 8, it can be seen that the skeleton curves of specimens SP1, SP2, and SP3 are similar before the maximum load is attained, but after yielding of the longitudinal bars the strengthened extent of specimen SP3 is larger than the other two specimens due to the larger amount of stirrups in the beam of SP3. As for the specimen SP1 with fewer stirrups, at large levels of displacement, the strength degenerates more obviously and earlier than that of SP2 and SP3.

Note that there exists a distinct difference between specimens SP4-SP6 and specimens SP1-SP3. SP4-SP6 show a relatively short post-yielded strengthened phase than that of SP1-SP3. The failure mode of SP4 and SP6 is obviously shear failure, and thus their strength degenerates earlier than the other specimens, and an increase in the amount of stirrups in the joint core regions leads to a reduction in strength degradation.

The experimental results of the key points for all of the skeleton curves are shown in Table 3, where the units of load and displacement are kN and mm, respectively, and the variables P_{cr} and Δ_{cr} respectively represent the load and the displacement of the specimens when the joint core region first cracked. From Table 3, the inter-story drift indices at the cracking point are in the range of 1/357~1/185 with an average value 1/230; the maximum values of the inter-story drift index are in the range of 1/31~1/25, and the average value is 1/28.

Table 3 Test results of key points in skeleton curves (kN, mm)

No.	P_{cr}	Δ_y	P_y	Δ_y	$P_{\max}$	$P_{\max}/P_y$	P_u	Δ_u	$P_u/P_{\max}$	Δ_u/Δ_y
SP1	30	7.00	29.32	6.96	40.9	1.40	35.5	47.55	0.86	6.83
SP2	27	6.85	27.50	7.14	40.35	1.47	36.25	48.35	0.90	6.77
SP3	27	8.10	26.0	7.30	43.1	1.65	36.55	56.0	0.85	7.67
SP4	28	4.20	42.5	8.55	59.05	1.39	51.16	56.7	0.86	6.63
SP5	30	6.7	40.45	9.13	59.25	1.46	51.7	58.8	0.87	7.20
SP6	35	6.56	39.7	8.00	60.45	1.52	51.0	58.9	0.84	7.36

4. Analyses of deformation components

4.1 Measuring method of each deformation components

In order to measure the following deformation components, such as the flexural and shear deformation in plastic-hinge regions, shear deformation in the joint core, and bond-slip of reinforcing bars in the beam-column joint, 14 electronic displacement transducers were installed on the critical regions of the subassemblages, which are shown in detail in Fig. 4 and Fig. 9.

No.1 to No.4 electronic displacement transducers installed longitudinally were used to measure the average curvature of the plastic-hinge region. By calculating the difference between the measured values of transducers No.7 and No.1 as well as the difference between the measured values of transducers No.4 and No.8, the slip of the longitudinal reinforcing bars in the joint core was obtained. Four transducers, No.9, No.10, No.13, and No.14, which were set along the diagonal direction, were used to measure the shear deformation in the critical region of the beam. No.11 and No.12 transducers were used to measure the shear deformation of the joint core region.

The installation devices of all the electronic deformation transducers noted above were elaborately

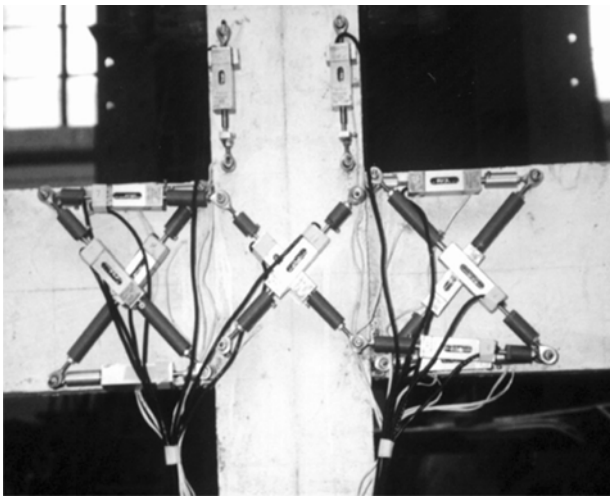

Fig. 9 Installation of electronic deformation transducers

designed and connected with universal bearings, which ensured that all these transducers could work well and that no accidental damage occurred in the transducers when the specimen produced large shear deformation or out-plane deformation.

4.2 Analysis model of each deformation components

The inter-story drift of a beam-column subassemblage Δ can be divided into three components, Δ_b, Δ_c, and Δ_j, as shown in Fig. 10, and the following equation can be obtained:

$$\Delta = \Delta_b + \Delta_c + \Delta_j \tag{1}$$

where Δ_b = the inter-story drift due to beam deformation;
Δ_c = the inter-story drift due to column deformation;
Δ_j = the inter-story drift due to shear deformation in joint core.

According to the geometrical relations shown in Fig. 10, the deformation component Δ_b can be determined by the following formula:

$$\Delta_b = \theta_b H = (\theta_{bp} + \theta_{slp} + \theta_{be} + \theta_{se})H/2 \tag{2}$$

where θ_{bp}= the plastic rotation angle of the plastic-hinge in the beam;
θ_{slp} = the rotation angle due to the slippage of longitudinal reinforcing bars in the joint;
θ_{be} = the elastic rotation angle of beam flexure deformation;
θ_{se} = the elastic rotation angle of beam shear deformation.

From the test results, it was found that the beam shear deformation contributed little to the total drift of the subassemblage, and therefore the influence of the beam shear deformation, θ_{se} could be neglected. θ_{bp} and θ_{slp} could be obtained from the test results, and the values of θ_{bp} and θ_{slp} at the ultimate state are shown in Table 4. In the present paper, the deformation of column Δ_c and the elastic rotation angle of the beam θ_{be} were calculated by elastic theory, where the concrete modulus

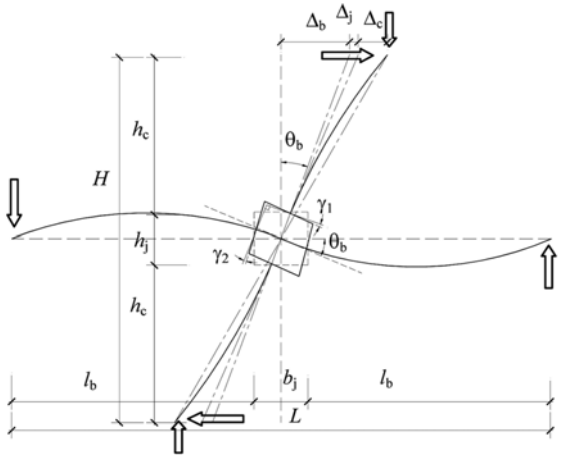

Fig. 10 The inter-story drift of a beam-column subassemblage

Table 4 Values of θ_{bp} and θ_{slp} at the ultimate state

	SP1	SP2	SP3	SP4	SP5	SP6
θ_{bp}	0.026	0.027	0.031	0.019	0.031	0.033
θ_{slp}	0.010	0.010	0.012	0.012	0.013	0.013

was taken as 85% of the original elastic modulus, so as to consider the influence of cracks and other plastic behavior.

The shear deformation rotation angle of the joint core region was calculated according to the deformation relations and the deformation values measured along the diagonal direction in the joint core. From the geometrical relations shown in Fig. 11, the shear deformation rotation angle γ could be obtained

$$\gamma = \gamma_1 + \gamma_2 \cong \frac{\sqrt{h_j^2 + b_j^2}}{h_j b_j} \frac{\delta_1 + \delta_2 + \delta_3 + \delta_4}{2} \tag{3}$$

where δ_1, δ_2, δ_3, and δ_4 are the tension and compression deformation of the joint core in the diagonal direction, which were directly measured by deformation transducers No.11 and No.12; h_j and b_j are the depth and width of the joint core, respectively.

With an assumption of $\gamma_1 = \gamma_2$ and the geometrical relations shown in Fig. 10, Δ_j could be calculated by formula (4):

$$\begin{aligned} \Delta_j &= 0.5H[\gamma_1(L - b_j)/L + \gamma_2(H - h_j)/H] \\ &= 0.25\gamma(2 - b_j/L - h_j/H)H \end{aligned} \tag{4}$$

where the denotations of the variables are shown in Fig. 10 and Fig. 11.

With the measured value, δ_1, δ_2, δ_3, δ_4 and the geometrical size of the joint core, the value of Δ_j at every loading stage could be calculated by formulas (3) and (4). By comparing the two calculated curves of SP4 and SP6 shown in Fig. 12, it is found that the amount of stirrups in the joint core had a large effect on the inter-story drift due to the shear deformation Δ_j.

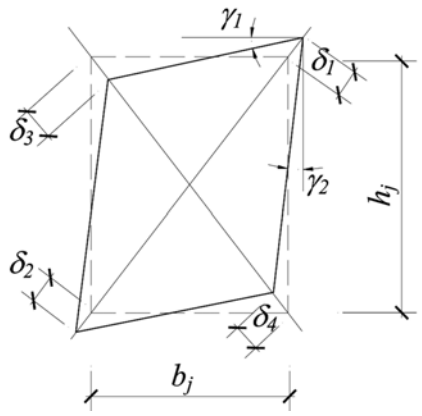

Fig. 11 Deformation of joint core

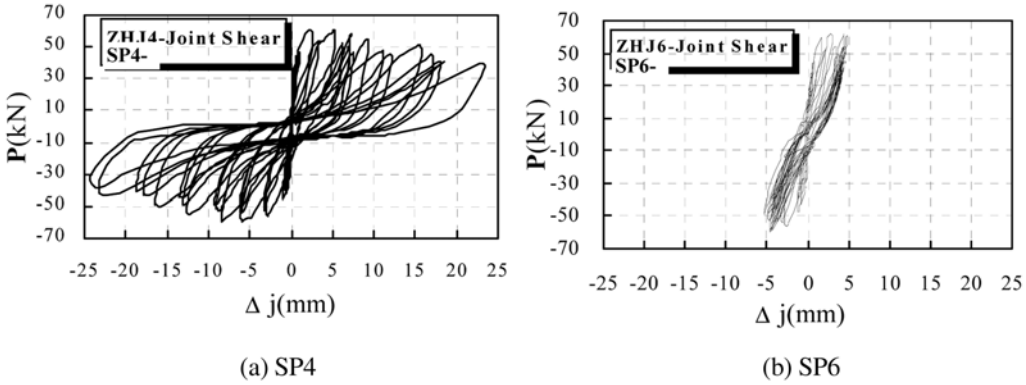

(a) SP4 (b) SP6

Fig. 12 Shear force-joint shear drift hysteretic relationships

For specimen SP4 (η_{cb} = 1.0), which finally failed in the joint shear failure mode, the drift due to shear deformation of the joint core was larger than that of any other specimens and showed an increase under subsequent cyclic loading with the same displacement amplitude (Fig. 12a). For specimen SP5 (η_{cb} = 1.10), with an increase of the amount of stirrups in the joint core, the drift due to shear deformation in the joint core reduced slightly. For specimens SP1, SP2, SP3, and SP6, which failed due to beam end bending failure, the drift due to the shear deformation was small and reduced at their unloading phase, which indicated that the joint still remained in the elastic range (Fig. 12b).

4.3 Contribution of different deformation components to global drift

Based on the above analysis and test data, the top drift caused by all the deformation components at each loading stage can be calculated. The contribution of each deformation component to the total drift as well as its changing pattern is shown in Fig. 13. For specimens SP1, SP2, SP3 and SP6, which failed in beam end bending failure mode, it is found that the contributions of the same type of deformation components to global drift are almost equal, and therefore an average value for these four specimens can be taken to represent the value of each deformation component contribution to the global drift of a subassemblage (Fig. 13a). Because SP4 failed in joint core shearing failure mode, the portions of each deformation component contribution to the global drift and the changing pattern of each component are quite different from those of subassemblages with a final failure mode of bending (Fig. 13b).

Test results indicate that the rotation due to bond-anchorage slippage is significant after the yielding of the longitudinal bars in the beam and with an increase of displacement amplitude the influence of slippage increases (See Fig. 13a). Many experimental studies on RC frame joints have indicated that the ratio of the bar diameter d_b to the column depth h_c has a large effect on the anchorage behavior of the longitudinal beam bars within the joint region. It is accordingly recommended that the d_b/h_c ratio be controlled as follows when designing a RC frame in seismic regions (Paulay and Priestley 1992):

$$d_b/h_c \leq 11/f_y \tag{5}$$

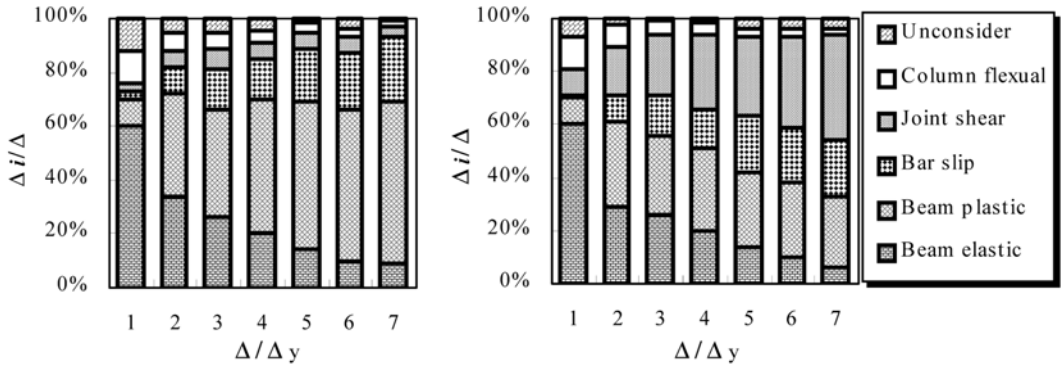

(a) Mean value of SP1, SP2, SP3 and SP6 (b) SP4

Fig. 13 Contribution of different deformation components to global drift

The specimen parameters d_b, h_c, and f_y in this paper are 12 mm, 200 mm, and 360 MPa, respectively. The d_b/h_c ratio of the specimens is 0.06, which is almost two times the control value recommended in the right of Eq. (5). Note that Eq. (5) is a design recommendation and thus may seem conservative. However, it is expected that a reduction in the d_b/h_c ratio of the specimens could lead to an improvement of the anchorage condition of the beam bars within the joint region, and the portion of drift due to anchorage slip could be reduced accordingly.

5. Conclusions

(1) It has been established that the final failure modes and hysteretic behavior are influenced by the strength ratio of joint to beam and column (η_{cb}). When the strength ratio, η_{cb}, is smaller than 1.33, a joint shear failure mechanism is likely to occur. It can be concluded that the appropriate strength ratio, η_{cb}, should be larger than 1.33 if the overstrength of the beam is not taken into account when assessing the required strength of the joint.

(2) For those specimens with a beam flexural failure mechanism, the portion of drift due to shear deformation of the joint is less than 7% under the entire loading history, and accordingly the shear deformation of joint can be ignored when performing an inelastic earthquake response analysis of RC frames. For those specimens with a joint shear failure mechanism, however, the contribution of shear deformation of the joint to the total drift can be even larger than that of the beam flexural rotation, and thus it cannot be ignored when a frame may experience a strong element-weak joint failure mechanism.

(3) Test results indicate that the rotation due to bond-anchorage slippage is significant after the yielding of the longitudinal bars in the beam and with an increase of displacement amplitude the influence of slippage increases. For those specimens with a beam end flexural failure mechanism, the percentages of drift due to bar slip deformation and beam flexural rotations to the total drift at the ultimate stage are about 24% and 60%, respectively, (see Fig. 13a).

(4) Based on the test results, the drift indexes when joint cracks occurred were about 1/357~1/185 and the mean value was 1/230. The drift index at the ultimate state ranged from 1/31 to 1/25, and the mean value of ultimate drift was 1/28.

Acknowledgements

This study was sponsored by the National Natural Science Foundation of China under Grant No.50478120 and Natural Science Foundation of Fujian Province, China under Grant No.E0410024.

References

Attaalla, S.A. and Agbabian, M. (2003), "Deformation characteristics of reinforced concrete beam-column joint cores under earthquake loading", *Advances in Struct. Eng.*, **6**(1), 15-21.

Bertero, V.V. and Popov, E.P. (1977), "Seismic behavior of reinforced concrete interior beam-column subassemblages", *ACI Publications* SP, **53**, 247-265.

Fenwick, R.C., Megget, L.M. and Wuu, P. (1996), "Load deflection characteristic of plastic hinges in ductile concrete beams", *Proc. 11th World Conf. on Earthq. Engrg.* Mexico, Paper No.469.

Paulay, T. (1988), "Seismic behaviour of interior beam-column joints in reinforced concrete space frames", *Proc. of Ninth World Conf. on Earthq. Eng.*, Tokyo Japan, Aug., 557-568.

Paulay, T. and Priestley, M.J.N. (1992), *Seismic Design of Reinforced Concrete and Masonry Buildings*, John Wiley & Sons Inc., New York.

Quintero-Febres, C. and Wight, J.K. (2002), "Experimental study of reinforced concrete interior wide beam-column connections subjected to lateral loading", *ACI Struct. J.*, **98**(4), 572-582.

Saatcioglu, M., Alsiwat, J.M. and Ozcebe, G. (1992), "Hysteretic of anchorage slip in RC members", *J. Struct. Eng.*, ASCE, **118**, 2439-2458.

Shin, M. and Lafave, J.M. (2004), "Modeling of cyclic joint shear deformation contributions in RC beam-column connections to overall frame behavior", *Struct. Eng. Mech.*, **18**(5), 645-669.

Teraoka, M., Hayashi, K. and Sasaki, S. (1998), "Behavior of interior beam-and-column subasemblages in an RC frame", *J. Fujita Technical Research Institute*, **9**, 9-23.

Teraoka, M., Kanoh, Y., Sasaki, S. and Hayashi, K. (1996), "Estimation of ductility in interior beam-column subassemblages of reinforced concrete frames", *Journal of the Society of Materials Science*, Japan, **45**(9), 1033-1041.

Zerbe, H. and Durrani, A. (1989), "Seismic response of connections in two bay RC frame subassemblies", *J. Struct. Eng.*, ASCE, **115**(11), 2829-2844.